Ice Growth Model for Polar Water Capture Systems

Beau M. Compton[1], Diane L. Linne[2], and Andrew J. Ring[3]
NASA Glenn Research Center, Cleveland, OH, 44135, USA

In-situ resource utilization (ISRU) is essential to NASA's goal of sustainable and cost-effective missions to the Moon and beyond. Water has become a particular source of interest since its discovery in the permanently shadowed regions (PSRs) of the Moon. This water exists as ice bound within the regolith, so one mode of capture is heating to sublimation temperatures and capturing at very low pressure. It then can be stored in ice form and transported out of the PSR and to a sunlit ridge, where processes such as electrolysis can be performed [2]. An understanding of frost growth dynamics under rarefied conditions is necessary for successful water capture and storage due to transient thermal properties of frost. A Diffusion-Limited Aggregation (DLA) approach was taken to analytically model bulk thermal conductivity changes of the growing frost layer under varying wall temperatures and frost layer porosities. The model utilizes well-known correlations for effective thermal conductivity and records the values as the frost layer thickness increases. This thermal conductivity can be applied to a known temperature change and be used to evaluate heat flux through the combined frost layer and tank wall for either a flat plate or cylindrical geometry. An experiment is described that will evaluate this model using one-dimensional frost growth on a horizontal, flat plate under low-pressure. The ice growth will be measured using a millimeter-scale photogrammetry camera system and a load cell measured transient mass growth.

I. Nomenclature

As	=	surface area
DLA	=	diffusion-limited aggregation
GRC	=	Glenn Research Center
ISRU	=	in-situ resource utilization
PSR	=	permanently shadowed region
q	=	heat flux
T	=	temperature
t	=	material thickness
κ_f	=	effective frost layer thermal conductivity
ρ_f	=	frost layer density

II. Introduction

The concept of extracting, processing, and utilizing local resources on foreign bodies is called in-situ resource utilization (ISRU). NASA is interested in using the ice bound in lunar regolith from the Moon's permanently shadowed regions (PSRs) to generate water for rocket propellant and life support. Studies from NASA indicate the potential for 5% water by weight to be bound within the soil [1]. Another study by NASA Glenn Research Center (GRC) developed a concept by which this ice can be excavated, baked into vapor form, stored in an ice tanker as a solid, and brought to the sun-lit regions of the Moon for electrolysis [2]. This concept in shown in Fig. 1.

The tanker used for storage will intake the water as a vapor from an auger-dryer system and quickly freeze it as frost, taking advantage of the cold surrounding environment [2]. The vapor is distributed to the inner surfaces from a thermally insulated distribution pipe. Because of the insulating effects of an increasing frost layer, it must be determined how thick the frost layer can grow before the reduced heat flux will preclude freezing of additional water vapor. Understanding of maximum frost layer thickness will then determine the amount of internal surface area the tank must have to ensure effective freezing of the desired quantity of water.

---

[1] AST, Propulsion Division.
[2] Senior Research Engineer, Propulsion Division, AIAA Associate Fellow.
[3] AST, Structural Mechanics Division.

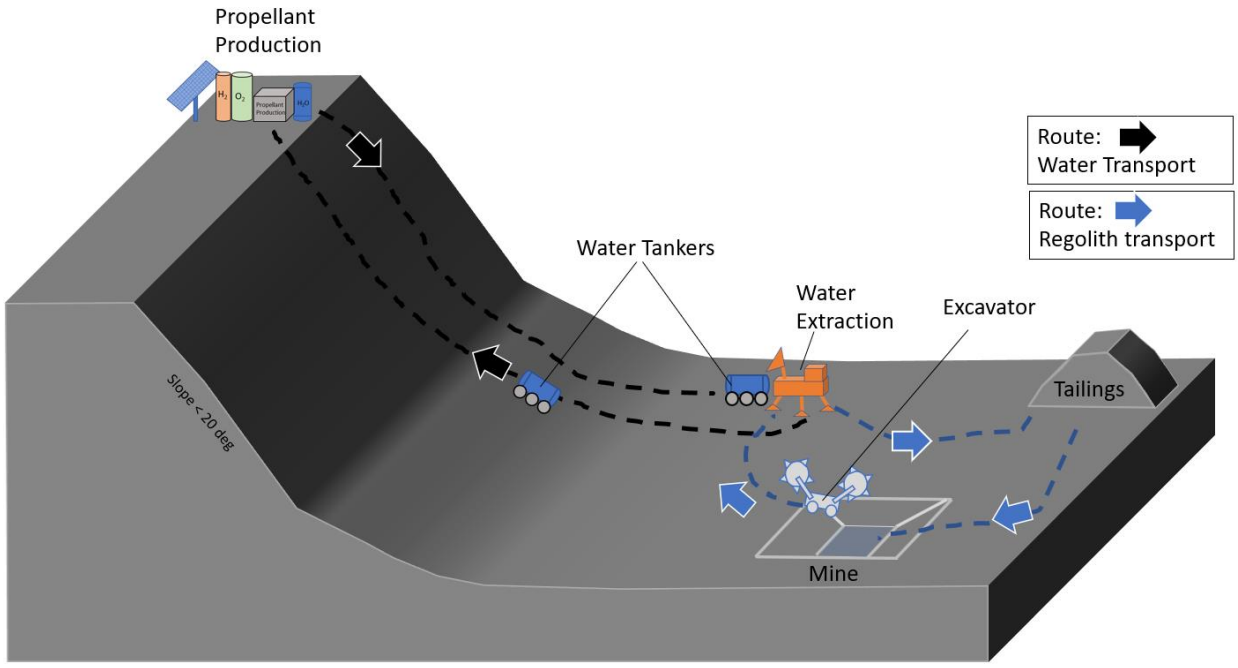


Fig. 1 Concept of operations of polar water plant.

Water vapor turns to frost via two modes: 1) condensation followed by freezing, and 2) desublimation. Both conditions require humid air cooled below the dew point and a cold surface. If the local conditions are below the triple point, then desublimation will occur directly, as shown in Fig. 2. Water vapor in the air cools in an isobaric manner and becomes supersaturated at the surface where phase change occurs. The vapor partial pressure becomes lower than that of the ambient air, creating a concentration difference that will drive frost formation [3]. Other factors such as contact angle, surface roughness, surface impurities, and air velocity also affect frost nucleation and growth [4].

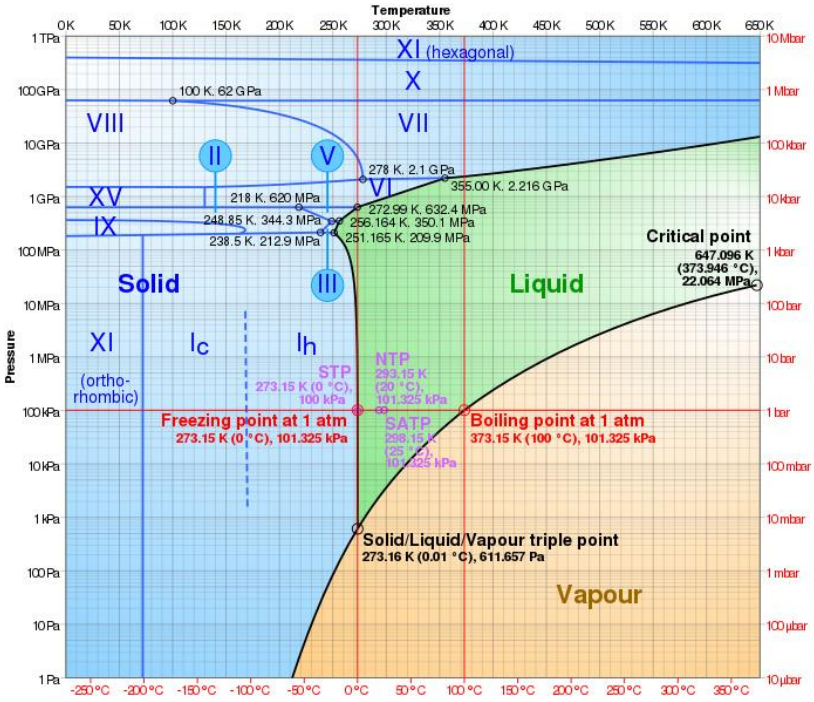


Fig. 2 Phase Diagram of Water [16].

The thermal properties of water in desublimation, though, are not fully understood. Most frost experiments do not operate under near-vacuum conditions and do not grow frost beyond a centimeter [5-8]. Many thermal conductivity studies also are limited in scope for these conditions [9-11].

What little research that has been done under low pressure indicates significant change in frost growth dynamics. It is shown in Ref. 5 that frost grows more slowly when subjected to 10,000 Pa due to a lower phase transition driving force. The morphology of the frost crystals also turned from irregular to columnar under 10,000 Pa and 50,000 Pa respectively, and the frost layer density decreased. These effects could have drastic impacts on the frost layer effective thermal conductivity and therefore the thermal performance. An important note of the study in Ref. 5 is that it operated above the triple point, meaning that phase transition included condensation. This could lead to drastically different results from the proposed desublimation frost growth in vacuum.

A diffusion-limited aggregation model has been used for frost growth by several researchers because diffusion is the main mode of mass transfer. Ref. 12 demonstrated the similarities of DLA modeling with experimental frost grown as low as -26 C. Ref. 13 used the fractal properties of the model to find a correlation for the thermal conductivity with porosity at wall temperature of -120 C and atmospheric pressure on a finned tube gassifier. Ref. 14 used a DLA model to calculate the thermophysical properties of frost that is sensitive to temperature and humidity.

In this paper a DLA model is described that predicts the frost growth at conditions below the triple point where the phase change moves directly from vapor to solid. A common correlation for thermal conductivity as a function of density is used. The model is used to predict maximum ice layer thickness and mass for a set of conditions specific to a conceptual lunar polar ice tanker. In addition, an experiment is described to gather the data necessary to validate this ice growth model.

III. Model Description

Heat flux throughout the frost layer is intrinsically tied to thermal conductivity via Fourier's law of thermal conduction:

$$q = -\kappa \nabla T \tag{1}$$

When applied to a flat surface with one dimensional heat flow in direction *x* the formula becomes:

$$q_x = -\kappa \frac{dT}{dx} \tag{2}$$

This can be applied to a simplified model of a frost layer with a thickness *t*, a linear temperature gradient, and an effective thermal conductivity κ_f:

$$q = \kappa_f \frac{T_f - T_w}{t} \tag{3}$$

Where T_w is the wall temperature (bottom of the frost layer) and T_f is the frost surface temperature.

When multiplying by the surface area, A_s, the heat transfer is:

$$Q = \kappa_f A_s \frac{T_f - T_w}{t} \tag{4}$$

This heat flux will initially start high due to a low porosity and frost layer thickness but will become increasingly lower through time. The temperature of the wall can be controlled through the design of the radiator; a higher radiator operating temperature (assumed equal to Tw) is desirable as it will result in a smaller and lighter radiator. To calculate heat flux as a function of time, relations for ice layer thickness, t, and effective thermal conductivity, k_f, must first be determined for various values of wall temperature and ice layer density.

A novel approach to modeling dynamic frost growth is through a diffusion-limited aggregation (DLA) model. DLA starts with vapor molecules in random motion above the flat plate. If a water vapor molecule touches an ice particle or the plate, it becomes "seeded" and part of the aggregate. After a molecule has become seeded or terminates due to leaving the control area, a new molecule is spawned. This process continues forming an aggregate frost layer with a porous structure like that of real frost. The model, written in MATLAB, has the capability to track the density,

porosity, and frost layer thickness as the aggregate grows. Thermal conductivity measurements were then calculated using a correlation from Ref. 10:

$$\kappa_f = 0.0140 + 0.00668\rho_f + 0.000175\rho_f^2 \tag{5}$$

Where ρ_f is the frost layer density. This correlation is not commonly used in forced convection conditions, though, so further assessment will need to be performed on its efficacy.

In the DLA frost-growth approach outlined by Ref. 14 the frost grows in three stages—the initial growth period followed by two alternating stages of growth and densification. For growth periods, the seeds are released from the top of the boundary which favors an increase in thickness and decrease in density. In the densification stage, seeds are only released within the frost layer which favors increasing density and stagnating thickness. A specified number of seeds are allowed to deposit in the initial growth stage. The model continues by alternating the growth stage and densification stage. A demonstration of frost growth is given in Fig. 3. The frost layer thickness is defined as the average of the highest and lowest peaks. In its current configuration, the model predicts a minimum density of approximately 350 kg/m^3 which occurs when skipping the densification stage. Additional cases can be run at different values of density by controlling the length of the densification stage.

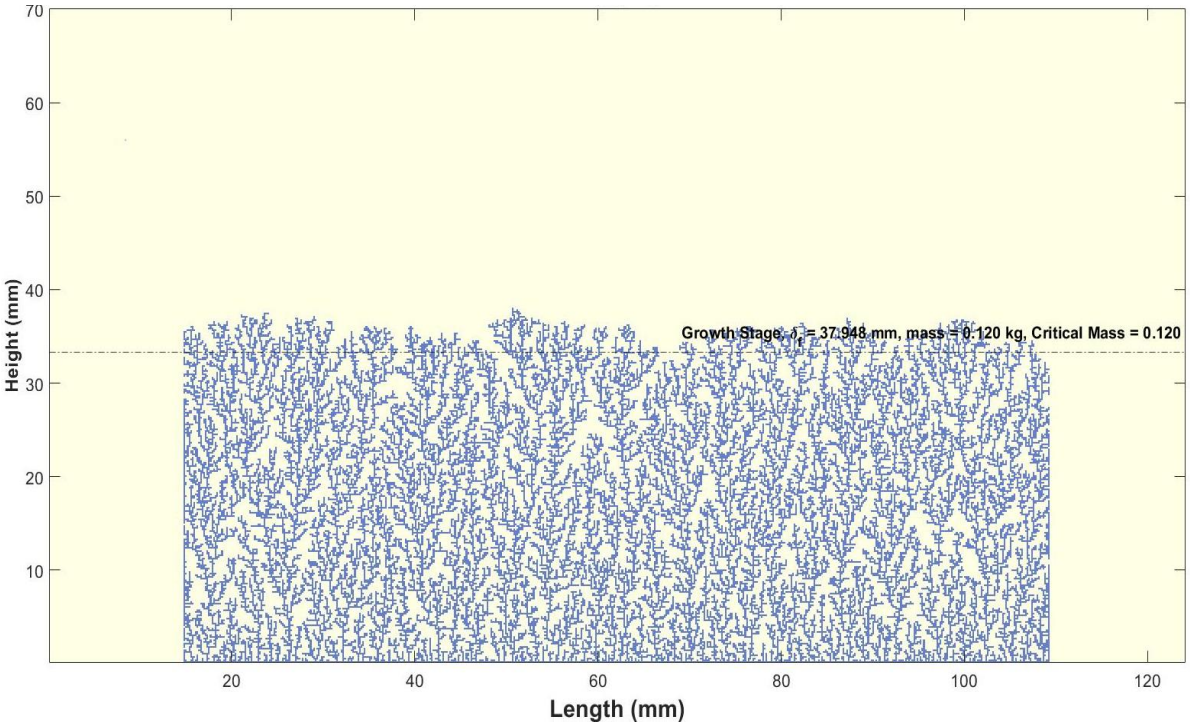


Fig. 3 Example of frost growth simulation using diffusion-limited aggregation model.

IV. Experimental Tests

To gather data to validate the DLA ice growth model, an experiment is planned where a 10-cm square flat plate will be chilled to temperatures in the expected range of the radiator operating temperature. A controlled water vapor stream will be introduced into the vacuum chamber and the change in ice thickness and mass will be measured over long durations. Density will also be calculated to allow for tuning of the model. The architecture study conducted at NASA GRC determined that approximately 116 W/m^2 of heat flux is required to capture the 0.22 kg/hr of water vapor from the pilot plant [2]. For the 10-cm flat plate tests, the mass flow rate was decreased to 0.0015 kg/hr to maintain the same heat transfer per unit area. This equates to 1.2 W of heat removed to continue to desublimate the incoming water vapor. Should the heat transfer drop below this value due to an increasing thermal resistance, vapor will no longer freeze.

A. Test Facility

All tests will be conducted in CW-14 at GRC. The stainless-steel chamber in Fig. 4 is 62 cm long and 41 cm in diameter. There are several vacuum flange ports throughout each side of the chamber. Three of these flanges have viewports attached for the photogrammetry measurements. Four flanges will be used for instrumentation feedthroughs and two flanges will be used for chilling fluid and water introduction. The chamber will be pumped down initially with a roughing pump and can be further pumped down via a diffusion pump. A recirculating chiller will be used to cool hardware inside the chamber to -40 C. At this temperature the chiller has a cooling capacity of 100 W, which is sufficient for the experiment.

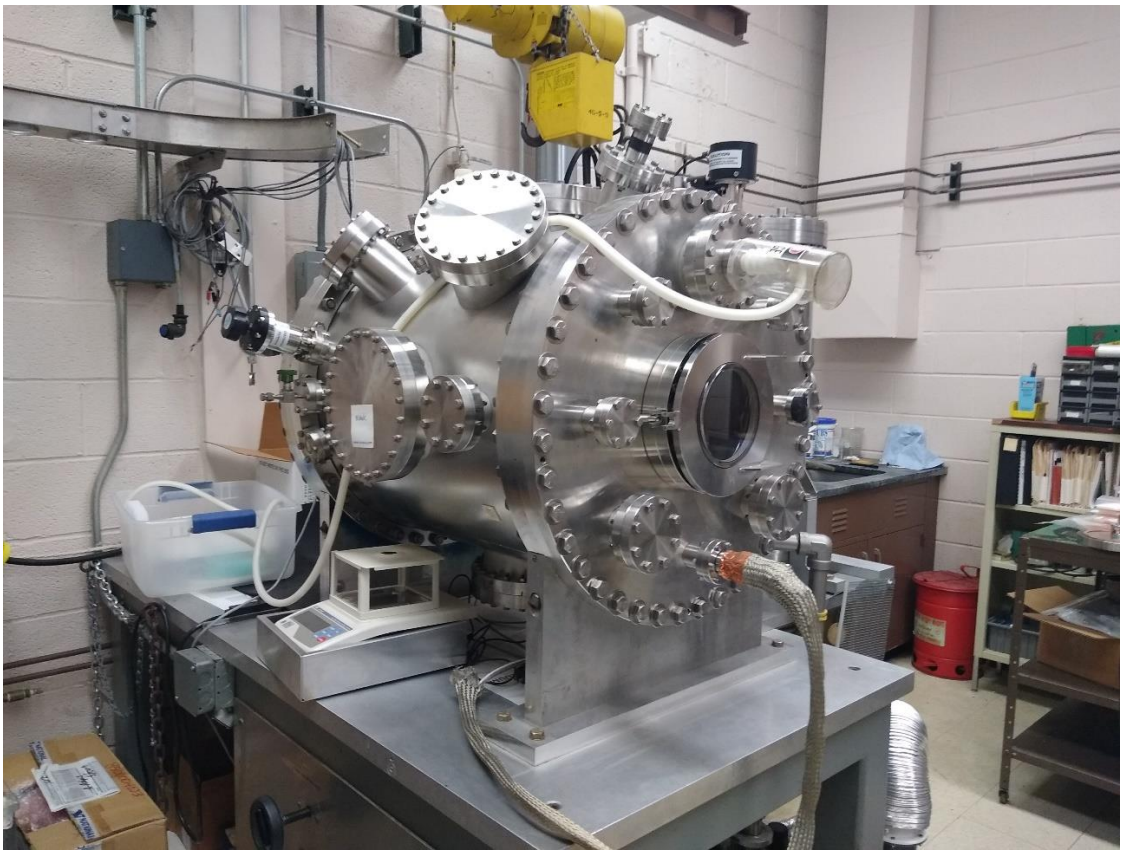


Fig. 4 Vacuum chamber to be used for the frost growth experiment.

B. Experimental Hardware

The set-up for the flat-plate experiment is shown in Fig. 5. Water will be introduced to the system via a zeolite molecular sieve bed. The zeolite will be loaded with water by flowing a saturated nitrogen stream through the bed at atmospheric conditions. The zeolite system will then be directed to the vacuum chamber, where the water will be released through a controlled temperature-pressure swing. The mass of the zeolite bed will be monitored during the test by a load cell to measure the mass flow rate into the test chamber.

The flat plate will be cooled with silicon fluid via a cooling plate to simulate the radiator operating conditions. The cooling plate will have six tube passes and has a 400 W cooling capacity. It will connect to the chamber feedthroughs via flex hoses which then connect to the recirculating chiller.

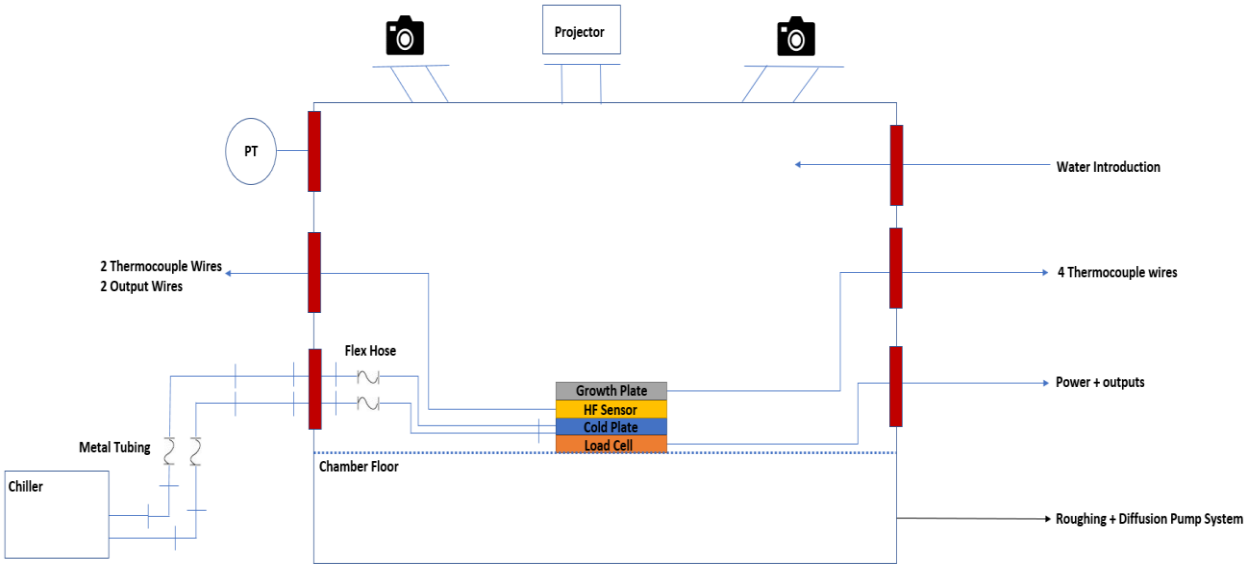


Fig. 5 Diagram of experimental setup.

The test plate used for the experiment will be 10 cm x 10 cm and made of aluminum 6061. Several type T thermocouples will be drilled into the plate for temperature measurement. Attached to the bottom will be a type T thermopile heat flux sensor with a 52 cm^2 sensing area with a sensitivity of 1500 $mV/W/cm^2$. A high-precision compression load cell will be placed below the cold plate to measure the changing mass of the frost layer.

A projector will be used to cast a stochastic pattern of black and white speckles through an optical port of the chamber and onto the surface of the frost for a brief period of time every 15 minutes. At the same time a stereo pair of cameras, mounted at optical ports viewing from an offset angle, will capture an image of the frost with the stochastic pattern on its surface. Using Digital Image Correlation (DIC) software, a 3-dimensional point cloud of the surface of the frost will be computed at each time interval, from which the amount of frost growth can be quantified. The concept is shown in Fig.6.

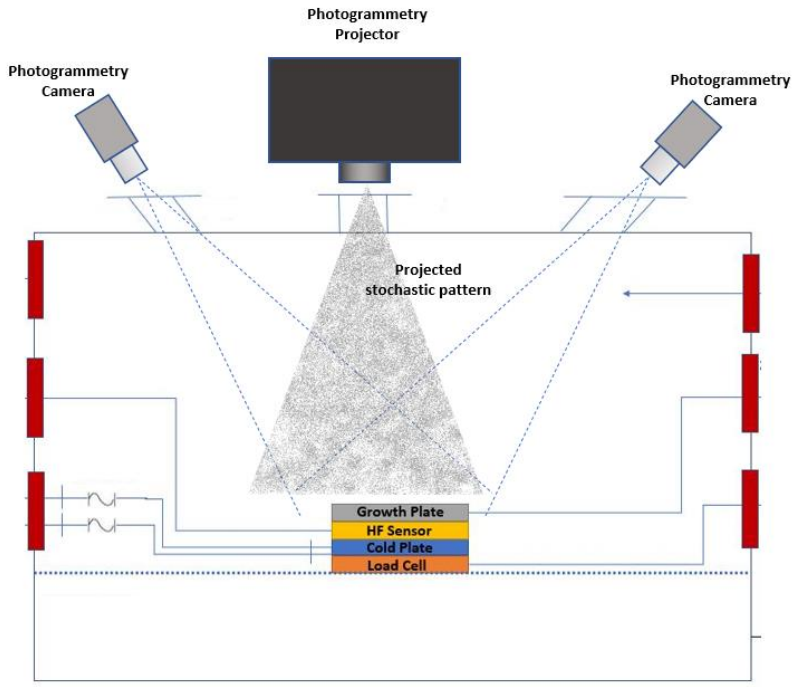


Fig. 6 Photogrammetry experimental setup.

C. Expected Results

The analytical model tracks the density of the frost layer as it deposits (Fig. 7). In the figure the density increases quite rapidly as the frost initially deposits and then converges on its minimum value of approximately 350 kg/m^3 (i.e., no densification stage).

Equation 5 shows that the effective thermal conductivity is closely tied to density. It follows the same trend as the density, with a sharp increase at the beginning followed by a convergence of around 0.410 W/m-K.

Equation 4 is used to calculate the heat flux through the frost layer. T_f is assigned as the melting point of the ice calculated at the local conditions of the frost layer. T_w will be held at different values creating several temperature differentials. As expected, the heat flux starts high as the frost layer is small and dense. As the frost layer grows, though, the heat rejected drops until it reaches the critical value of 1.2 W. The frost thickness, mass, and time can then be recorded for the different values of delta-temperature. Results show that the max ice thickness is highly sensitive to ΔT, ranging from 7.8 mm to 38.4 mm for a temperature difference of 2 K and 12 K, respectively.

To understand how the density affects the prediction of critical ice layer thickness for a desired heat flux, Fig. 8 shows the heat flux as a function of frost thickness for different densities at a delta-temperature across the layer of 7 K. Results show that densities varied from 350 to 450 kg/m^3 have a moderate impact on maximum frost layer thickness, from 23.3 mm to 30.9 mm, respectively.

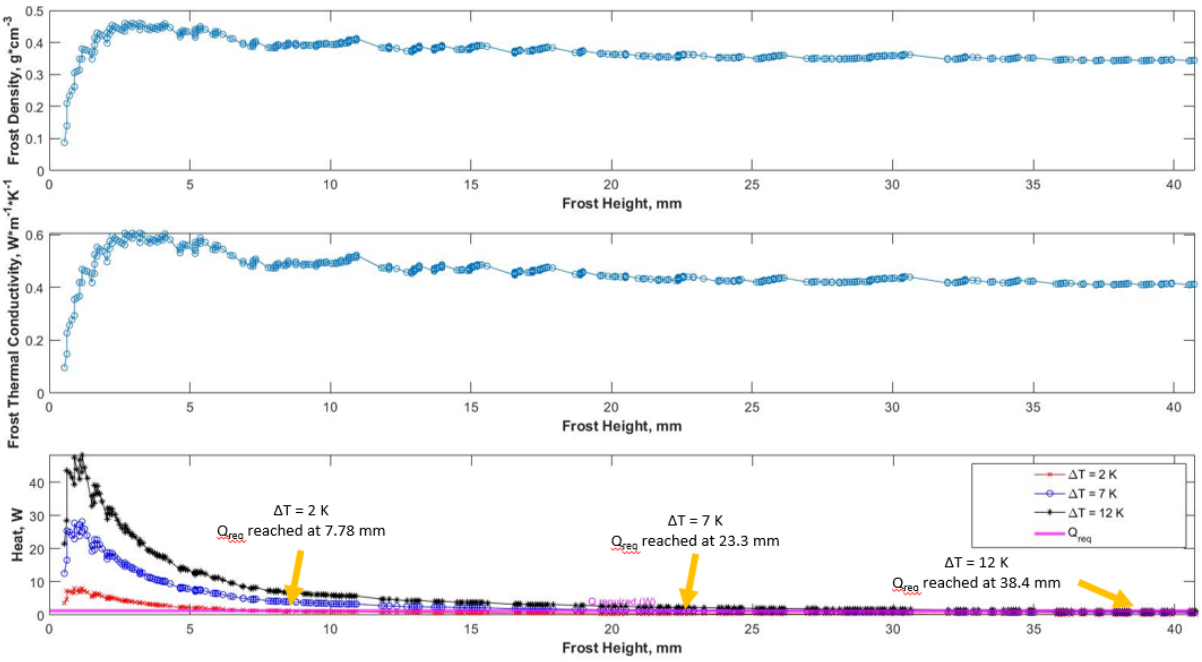


Fig. 7 Frost density, effective thermal conductivity, and heat as a function frost thickness.

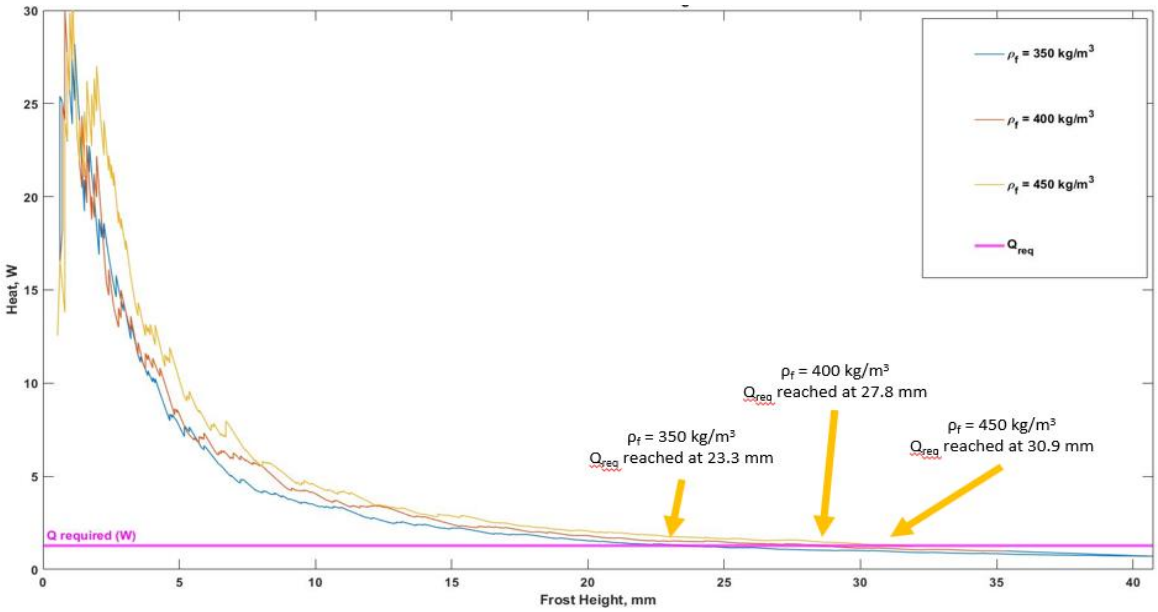


Fig. 8 Heat removed as a function of frost height with varying frost densities.

V. Summary

Understanding the dynamics of a growing frost layer in rarified conditions is crucial for the success of water capture on the lunar surface. In the ice tanker, a growing frost layer suggests an increasing thermal resistance which the passive radiator eventually cannot match. A model written in MATLAB uses a novel DLA approach to predict the heat flux throughout the frost layer as a function of frost thickness and mass. Once the critical predicted heat flux is reached there will be insufficient heat removal to continue to capture the incoming water vapor. A common correlation is used to evaluate the effective thermal conductivity of the frost layer, which is only a function of frost density. The density can be manipulated for the model to fit varying environmental conditions. Several assumptions were used in this model, including: (1) a constant temperature for the frost surface and the wall temperature, (2) no convective or radiative heat transfer in the frost layer, (3) All water vapor freezes as soon as it is exposed to the growth plate, (4) heat and mass transfer within the frost layer is one-dimensional and quasi-steady, and (5) the density and thermal conductivity are uniform over the frost thickness. The first assumption is the most important to consider so further research will be needed to evaluate its impact.

References

[1] Colaprete, A., et al, 2010, "Detection of Water in the LCROSS Ejecta Plume," Science, 22, 463-468.
[2] Linne, D., Kleinhenz, J., and Paz, A., 2020, "Lunar Water Pilot Plant Conceptual Design," AIAA 2020-4236, Nov. 2020.
[3] Sun B., Ghatage S., Evans G. M., Bhatelia T., Utikar R., and Pareek V. K., 2020, "Dynamic study of frost formation on cryogenic surface," International Journal of Heat and Mass Transfer, 150
[4] Na, B., and Webb, R., 2003, "A fundamental understanding of factors affecting frost nucleation," International Journal of Heat and Mass Transfer, 46, 3797–3808.
[5] Chen, Y., Lu, P., Shen, C., and Zhang, Q., 2015, "Experimental study on frost formation on a cold surface in low atmospheric pressure," Applied Thermal Engineering, 90, 86-93.
[6] Liu, S., Jiao, W., Ren, L., Tian, and X., 2020, "Thermal resistance analysis of cryogenic frosting and its effect on performance of LNG ambient air vaporizer," Renewable Energy, 149, 917-927.
[7] Cheikh, A., and Jacobi, A., 2014, "A mathematical model for frost growth and densification on flat surfaces," International Journal of Heat and Mass Transfer, 77, 604-611.
[8] Hermes, C. J. L, Piucco, R. O., Barbosa Jr., J. R., and Melo, C., 2009, "A study of frost growth and densification on flat surfaces," Experimental Thermal and Fluid Science, 33, 371-379
[9] Sahin, A. Z., 2000, "Effective thermal conductivity of frost during the crystal growth period," International Journal of Heat and Mass Transfer, 43, 539-553.
[10] Yonko, J. D., and Sepsy, C. F., 1967, "An Investigation on the Thermal Conductivity of Frost While Forming on Flat Horizontal Plate," ASHRAE Transactions, 73, 1.1-1.11.
[11] Negrelli, S., and Hermes, C. J. L., 2015, "A semi-empirical correlation for the thermal conductivity of frost," International Journal of Refrigeration, 58, 243-252.

[12] Yaomin, L., Zhongliang, L., and Lingyan, H., 2012, "Experimental and theoretical investigations of the fractal characteristics of frost crystals during frost formation process," Experimental Thermal and Fluid Science, 36, 217-223.
[13] Chen, S., Yao, S., and Xie, F., 2013, "Analysis of Thermal Conductivity of Frost on Cryogenic Finned-tube Vaporizer Using Fractal Method," Energy and Power Engineering, 5, 109-115.
[14] Negrelli, S., Cardoso, R. P., and Hermes, C. J. L., 2016, "A finite-volume diffusion-limited aggregation model for predicting the effective thermal conductivity of frost," International Journal of Heat and Mass Transfer, 101, 1263-1272.
[16] https://commons.wikimedia.org/wiki/File:Phase_diagram_of_water.svg